Temporally Harmonic Oscillons in Newtonian Fluids

H. Arbell and J. Fineberg

The Racah Institute of Physics, The Hebrew University of Jerusalem, Jerusalem 91904, Israel

(Received 18 January 2000; revised manuscript received 29 March 2000)

Stationary, highly localized (oscillon) structures are observed in a Newtonian fluid when nonlinear surface waves are parametrically excited with two frequencies. Oscillons have a characteristic structure, that of periodically self-focusing jets. In contrast to previously observed oscillons in highly non-Newtonian media, these states are temporally harmonic with the forcing. For wave amplitudes greater than a critical value, they nucleate from an initial pattern via a hysteretic bifurcation, and can therefore be localized on a background of patterns with a variety of different spatial symmetries.

PACS numbers: 47.54.+r, 05.45.Yv, 47.20.Gv, 47.35.+i

Highly localized structures have recently been observed in a number of 2D uniformly driven nonlinear pattern-forming systems. In contrast to states which are strongly localized solely in the direction normal to the pattern's wave vector (see, e.g., Refs. [1–3]), oscillon states, which are nearly stationary circular regions that oscillate between conical peaks and craters, are strongly localized in all directions, with no internal structure. Although these intriguing particlelike states have now been observed in two distinct nonlinear systems [4,5], basic features such as their localization mechanism [6–9], form, and generality are not yet understood. Here we quantitatively describe highly localized states, appearing in a Newtonian fluid, whose form is qualitatively similar to oscillons. The basic mechanism for their formation is described.

Oscillons have been recently observed in both granular media [4] and colloidal suspensions [5] subjected to a spatially uniform acceleration, $g_z \sin\omega t$, parallel to $\vec{g}$. With this excitation, the surface of both of these highly non-Newtonian systems becomes unstable (the Faraday instability) via a subcritical bifurcation to a standing wave pattern with a subharmonic frequency, $\omega/2$. Oscillon states are observed in the hysteretic region, where both patterns and featureless "flat" states are bistable.

Oscillons have also been observed in a number of spatially continuous models of subcritical systems. As in experiments, Swift-Hohenberg equations [6,7], a complex Ginzburg-Landau equation coupled to an auxiliary field [8], and subcritical period-doubling maps with continuous spatial coupling [9] have all yielded temporally subharmonic oscillons that appear *solely* in the bistable region of phase space, where both patterns and featureless states can be stable. Subharmonic temporal response, together with bistability, was therefore assumed to be a necessary condition for oscillon formation [7]. Below, we will demonstrate that *temporally harmonic* states similar in spatial structure to previously observed oscillons can form well *beyond* the bistable region of a pattern. Because of the marked similarity of their form, we will also refer to these new states as oscillons (or "harmonic oscillons" where possible ambiguity may arise). Harmonic oscillons can concurrently coexist with either featureless or patterned states having a variety of spatial symmetries. Oscillon dynamics influence the overall coherence of the underlying patterns and may affect transitions between order and spatiotemporal complexity. Their existence in *Newtonian* fluids may indicate that oscillon formation is independent of any particular (e.g., shear-thinning) rheological property of their support.

In the experiments described below, we generate oscillons via spatially uniform vertical acceleration of a Newtonian fluid layer of depth h with two commensurate frequencies, $\omega_1 = m\omega_0$ and $\omega_2 = n\omega_0$, where $n > m$ are mutually prime integers. In the forcing function,

$$g_{dr} \equiv g_z[\cos(\chi)\cos(m\omega_0 t) + \sin(\chi)\cos(n\omega_0 t + \phi)], \tag{1}$$

the angle χ describes the degree of mixing between modes with critical wave numbers, and k_1 and k_2 correspond, respectively, to ω_1 and ω_2.

Our working fluids were Dow-Corning 200 silicone oils with kinematic viscosities, ν, of 8.7, 23, 47, 87 cS (1 cS $\equiv 10^{-2}$ cm^2/s). Experiments were performed in circular fluid layers of diameter 14.4 cm with $0.15 < h < 0.55$ cm, where pattern correlation lengths [10] are typically much less than the system size. Oscillons were observed using frequency combinations $n : m = 3 : 2$ and $5 : 4$ with $10 < \omega_0/(2\pi) < 35$ Hz and $10 < \omega_0/(2\pi) < 20$ Hz, respectively. The oscillon patterns generated were both stable for $-50° < \phi < +50°$ and in three-frequency forcing of 1:2:3 and 2:3:4. In experiments with frequency combinations (in Hz), 50/25, 60/30, 80/40, 56/40, 63/45, 68/48, 70/50, 75/55, 77/55, 50/30, 70/40, 60/45, 65/50, 80/50, 68/52, 84/60, and 100/60 oscillon states were *not* observed. The experimental system, consisting of a computer-controlled electromagnetic shaker and visualization system, was described in detail in [11]. Visualization of pattern and oscillon states was performed both from above, using the gradient visualization scheme

 0031-9007/00/85(4)/756(4)$15.00

described in [11] and via direct visualization from the side with shutter speeds of 0.1–1 ms, enabling measurement of instantaneous amplitudes.

In Fig. 1a we present a typical time sequence of a single oscillon, on the background of a flat underlying state. Similar states had been previously noted in [12]. In contrast to previously observed subharmonic oscillons, the oscillon period, $2\pi/\omega_0$, is *harmonic* with the basic forcing frequency. A typical phase space for a 3:2 forcing ratio is shown in Fig. 1b. Oscillons typically appear near the bicritical point, where states corresponding to both ω_1 and ω_2 are concurrently unstable. As described in [10,11,13] square (hexagonal) patterns correspond to regions of phase space dominated by response frequencies that are subharmonics (harmonics) of ω_0. Oscillons are formed only in regions of phase space where the *harmonic* frequency is dominant. On a subsequent change of either g_z or χ, however, they can persist in narrow regions on the subharmonic side bicritical point as, for example, when coexisting with squares (see Fig. 1).

Oscillons (Fig. 1c) can be surrounded by patterns having a number of different symmetries. When surrounded by squares, the oscillons and squares oscillate with respective angular frequencies of ω_0 and $3\omega_0/2$. Oscillons (Fig. 1c, right) are also observed in a large area of phase space on a background of a superlattice state formed by two superimposed hexagonal lattices (labeled hexagonal-based oscillons or HBO) with a relative orientation of $22° \pm 2°$. In the center of each superhexagon a large amplitude oscillon is present while the nearest neighbors have smaller amplitudes. This state is qualitatively similar to superlattice I states observed in [14,15]. When surrounded by a flat state, oscillons are metastable with typical lifetimes of 10^3–10^4 oscillation periods. The amount of both hysteresis and lifetimes of the oscillon states increases with the fluid viscosity.

Oscillons are readily discerned within many different patterns such as the twelvefold quasipatterns formed in a 5:4 forcing ratio (Fig. 2b) and spatially subharmonic superlattice (SSS) states (Fig. 2c). Although not easily apparent from above, the high-amplitude characteristic form of oscillons within these patterns is readily seen when the state is viewed from the side. In contrast to the temporally harmonic response of the oscillons when surrounded by either the flat or hexagonal states, oscillons surrounded by SSS states [11] echo the temporally subharmonic response observed in these patterns. Spatially, this response is seen as a lateral shift of the oscillons' position every $2\pi/\omega_0$.

Multifrequency oscillons can, as in [4,5], form bound states such as the doublet and triplet shown in Fig. 2a. As the fluid viscosity is increased there is more of a tendency to form multioscillon bound states with a larger number of components (Fig. 2d). This suggests that the attractive force between oscillons increases with ν. Within bound states all of the component oscillons are *in phase* with one another. In contrast to single-frequency oscillons where larger structures are created with increased driving, two-frequency oscillons on a flat background are destabilized by an increase in the driving amplitude. When located within a pattern, however, increased driving amplitude generally results in the creation of a larger number of oscillons and, for high driving amplitudes, droplet ejection.

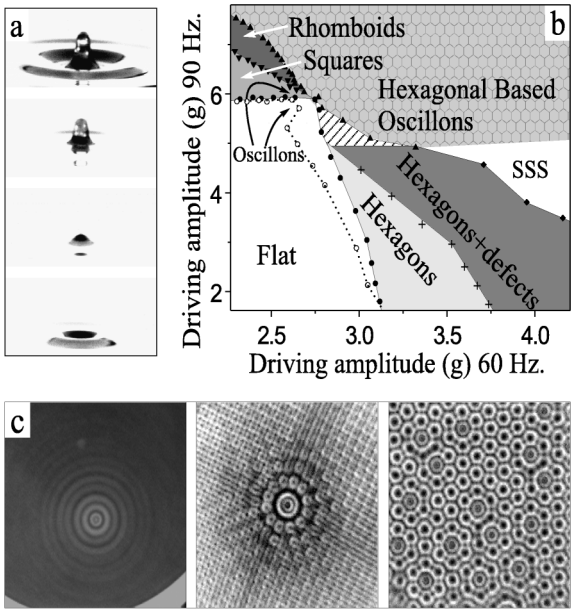

FIG. 1. (a) A time sequence of an oscillon observed at $\omega_0/(2\pi) = 25$ Hz, $\nu = 47$ cS, and $h = 0.33$ cm. The frames, of width 1.6 cm, are 6.7 ms apart. (b) A typical phase diagram [$\omega_0/(2\pi) = 30$ Hz, $h = 0.2$ cm, $\nu = 23$ cS]. Besides the square, hexagon, SSS, and rhomboid states reported previously [13], we observe oscillons (whose locations are indicated by the dark arrows) that can coexist with the flat state [(c) left) at $\nu = 47$ cS, $\omega_0/(2\pi) = 25$ Hz, and $h = 0.35$ cm; square state and hexagonal-based oscillon state [(c) center and (c) right] at $\omega_0/(2\pi) = 30$ Hz and $h = 0.2$ cm. Filled (open) symbols describe transition lines measured for fixed χ and increasing (decreasing) g_z. The hatched region is a transition region between hexagonal and HBO patterns. All states were obtained with a 3:2 forcing ratio and $\phi = 0°$.

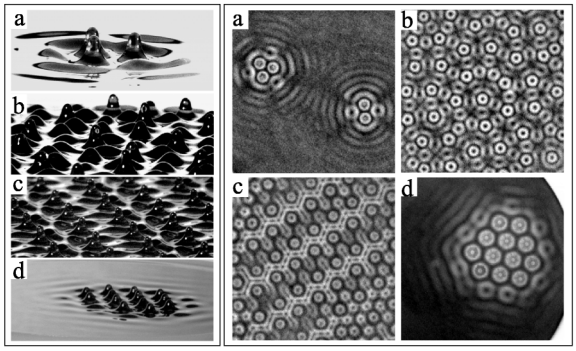

FIG. 2. Typical oscillons within a (a) flat state ($\nu = 47$ cS, 75/50 Hz); doublet and triplet (right) at $h = 0.4$ cm and a triplet (left) at $h = 0.33$ cm. (b) Twelvefold quasipattern at $\nu = 47$ cS, 75/60 Hz, $h = 0.33$ cm. (c) An SSS pattern ($\nu = 23$ cS, 75/60 Hz, $h = 0.2$ cm). (d) A localized hexagonal oscillon structure ($\nu = 87$ cS, 60/40 Hz, $h = 0.4$ cm).

An oscillon's width and maximal amplitude scale differently. The maximal amplitude scales roughly as 0.35λ, where λ is the wavelength of the underlying pattern. In contrast, the oscillon width is nearly constant, decreasing less than 30% for a factor of 3 change in λ with only slight dependence on both h and ν. The surrounding ripples are damped with a (ν-dependent) $(2-5)\lambda$ radial extent.

Let us now consider the transition from a spatially extended state to oscillons. In Figs. 3a–3d we plot the (temporally harmonic) hexagonal pattern amplitude as a function of the forcing $g_z \cos\chi$ (corresponding to $m\omega_0$) for different fixed values of the second driving amplitude, $g_z \sin\chi$ (corresponding to $n\omega_0$). The patterns first undergo a hysteretic bifurcation from the flat state, with the amount of hysteresis an increasing function of $g_z \sin\chi$. The pure hexagonal state can be empirically described by an amplitude equation of the form

$$dA/dt = \epsilon A + BA^{\dagger 2} - \gamma|A|^2 A, \qquad (2)$$

where $B \propto g_z \sin\chi$, $\epsilon \equiv (g_z \cos\chi - g_z \cos\chi|_c)/g_z \cos\chi|_c$ is the reduced driving amplitude, with $g_z \cos\chi|_c$ the hexagon threshold. The third order coefficient, γ, is constant to within 20% as $g_z \sin\chi$ is varied. The hexagonal pattern, for all values of $g_z \sin\chi$, loses stability at the *same* critical value, H_c, of the pattern amplitude. $H_c \propto \lambda$, where λ is the hexagon wavelength. $H_c = 0.17\lambda$ for $h = 0.2$ cm, $\nu = 23$ cS, and $15 < \omega_0/(2\pi) < 35$ Hz. These transition points, in the phase diagram, typically lie along a straight line for 3:2 forcing [Figs. 3 (left) and 1b], a fact consistent with Eq. (2).

As indicated in Fig. 3, for low values of $g_z \sin\chi$ oscillons are not seen. Nonhysteretic transitions at H_c, instead, occur to a hexagonal pattern marked by sporadic high-amplitude defects. These defects, like the oscillon states, initially form near the lateral boundaries. For increased driving amplitudes, defects are not confined to the boundaries and can nucleate throughout the entire system. We surmise that the transition at H_c corresponds to a shape-changing instability of the underlying pattern. Similar transitions from low- to high-amplitude states with qualitatively different shapes have been observed in suspended fluid drops (pendant drops) when either sinusoidally forced [16] or static [17]. Transitions leading to droplet ejection at a critical wave amplitude proportional to λ also occur in both forced gravity and capillary waves [18,19].

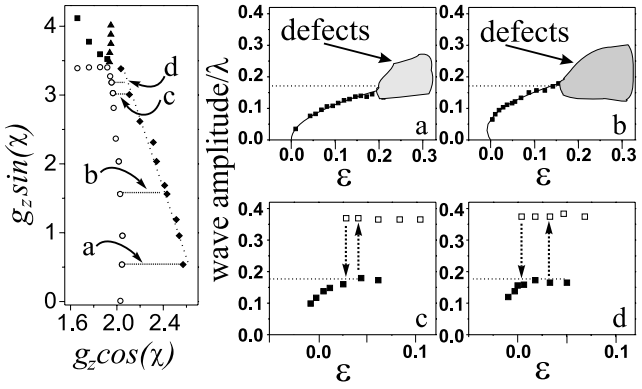

FIG. 3. (Right) The hexagonal pattern amplitude (filled squares) ($\nu = 23$ cS, $h = 0.2$ cm, and 60/40 Hz forcing) as a function of the reduced 40 Hz forcing amplitude, ϵ, for 60 Hz forcing amplitudes, $g_z \sin\chi$, of (a) 0.54 g, (b) 1.56 g, (c) 3.03 g, and (d) 3.18 g. At a critical amplitude of $H_c = 0.17\lambda$ (dotted lines) a transition occurs to either oscillons [open squares in (c) and (d)] or high-amplitude defect states [(a) and (b)]. (Left) Phase space with the locations of H_c (diamonds) and measurement intervals corresponding to (a)–(d) noted. Transitions to the primary instability (open circles), rhomboids (squares), and HBO states (triangles) (see Fig. 1) are noted.

The transition to oscillons at H_c elucidates a number of their characteristics. A pattern can *generate* an oscillon when any *local* amplitude becomes greater than H_c. Thus, as in Fig. 2, oscillon locations within a given pattern correspond to the pattern's local maxima. Thus a superlattice state formed by two superimposed hexagonal lattices with a relative orientation of 25° produces oscillon doublets, while a relative orientation of 40° produces more triplets. This also explains why the *number* of oscillons increases with the driving amplitude (as the wave amplitude surpasses H_c at more locations), while oscillon amplitudes (Figs. 3c and 3d) stay relatively constant.

Figure 3 highlights an important feature of oscillons; they bifurcate to a distinct branch *above* the patterns that generate them. The region of bistability of the two branches is a function of $g_z \sin\chi$. Depending on their relative saddle node locations, oscillons can appear either localized on a flat background (close to Fig. 3d) or can decay to the hexagonal state (Fig. 3c). The pure hexagon branch (Fig. 1b) is not observed near the bicritical point because, as Eq. (2) indicates, for large $g_z \sin\chi$ the growing *transient* hexagon amplitudes surpass H_c, generating oscillons *before* steady-state hexagons are reached.

What mechanism leads to oscillon formation? A necessary condition for oscillon formation is that a pattern arrive at the critical wave amplitude, H_c, where an instability occurs to either large amplitude defects or oscillons. Large amplitude defects differ from oscillons as they are transient with lifetimes (of order π/ω_0) and peak amplitudes, both significantly lower than oscillons and about 20%–60% higher than the surrounding waves. We now present evidence that the oscillons described here are essentially local jets, similar to jets formed by inertial collapse of axisymmetrically displaced fluid as in [20,21]. A falling drop, or, in our case, a high amplitude wave accelerating into the fluid, creates a craterlike deformation upon impact with the fluid surface. Under the action of gravity (or positive acceleration of the plate) the crater then collapses radially inward. This focuses kinetic energy and creates a high-energy jet along the crater axis. Zeff *et al.* [20] have shown that this occurs in deep fluids when parametrically forced surface waves, upon reaching a critical amplitude, collapse to a finite-time singularity of both the energy density and the velocity field along the axis. Similar phenomena occur when fluid drops fall from above a critical height [21]

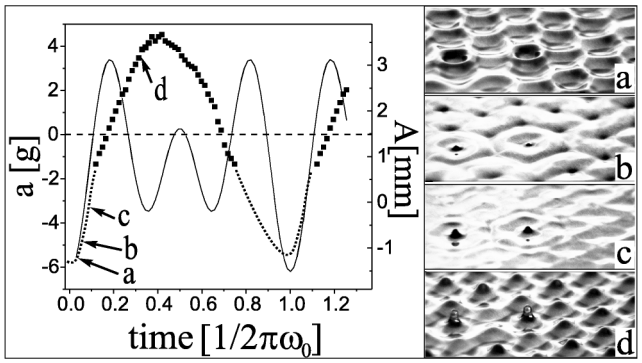

FIG. 4. (Right) Images of representative temporal phases of two typical oscillons (at 60/40 Hz driving) within a hexagonal pattern. As the crater phase (a) collapses, thin jets are formed (b),(c) which then develop into thick jets (d). (left) The peak amplitude of an oscillon (squares) as a function of time over a single excitation period, $2\pi/\omega_0$, compared to the total acceleration, $a = -(g + g_{dr})$ (solid line). Amplitudes noted by the dotted line were hidden by the cell's lateral boundary and are approximate.

into a fluid. When the fluid is shallow, interaction with the lower boundary [22] leads to thick jets, similar in form to oscillons.

The detailed dynamics of oscillons support this idea. Photographs (Figs. 4a–4d) of representative temporal phases of two oscillons within a hexagonal pattern show that as a well-defined crater phase (Fig. 4a) collapses thin jets are first formed (Fig. 4b) that then develop into the thick jets that we recognize as oscillons. Comparison of an oscillon peak with the instantaneous driving acceleration [Fig. 4 (left)] supports this picture. Oscillon time dependence is asymmetric, with growth much more rapid (20%–30% of a period) than decay. Significantly, rapid growth occurs well *before* positive total acceleration, $a = -(g + g_{dr})$, with the first measurable velocities significantly (50%–80%) higher than both the surface wave group velocity and maximum plate velocity. These effects suggest crater collapse.

Figure 4 shows the oscillon to be efficiently pumped by the system. A local maximum of the plate acceleration at an oscillon's peak (i.e., maximum effective gravitational potential) and maximal relative velocity when the oscillon and fluid surface merge (at $A = 0$ in Fig. 4) yield efficient crater formation. Optimal inertial collapse of the crater *rim* is achieved by maximal plate acceleration (point *a* in Fig. 4) at the crater phase. Optimal pumping cannot always be achieved, as the oscillon growth rate provides an intrinsic time scale. This may explain why oscillon states are not observed for all values of ϕ or $n : m$, which govern the form of the driving function.

In conclusion, oscillon states whose time dependence is temporally harmonic with the forcing frequency can exist in Newtonian fluids. Unlike previously observed oscillon states, they do not solely appear in a region of bistability of two global states, but rather bifurcate subcritically from a pattern at critical wave amplitude to a *distinct* branch. This bifurcation can lead to either transient high-amplitude defects that sporadically form throughout the pattern or, for higher wave amplitudes, to oscillons. Harmonic oscillons are periodically self-focusing jets that can be localized within states with a variety of different spatial symmetries. As the structure of previously observed oscillons is also qualitatively similar to these jets, we surmise that they may be generated by a similar mechanism. In contrast to other suggested localization mechanisms [7], this model may explain the selection of oscillons' highly localized, characteristic shape.

We acknowledge the support of the Israel Academy of Sciences (Grant No. 203/99).

[1] E. Moses, J. Fineberg, and V. Steinberg, Phys. Rev. A **35**, 2757 (1987); R. Heinrichs, G. Ahlers, and D. S. Cannell, Phys. Rev. A **35**, 2761 (1987).
[2] M. Dennin, G. Ahlers, and D. Cannell, Science **272**, 388 (1996).
[3] H. Riecke and G. D. Granzow, Phys. Rev. Lett. **81**, 333 (1998).
[4] P. Umbanhowar, F. Melo, and H. L. Swinney, Nature (London) **382**, 793 (1996).
[5] O. Lioubashevski, Y. Hamiel, A. Agnon, Z. Reches, and J. Fineberg, Phys. Rev. Lett. **83**, 3190 (1999).
[6] H. Sakaguchi and H. R. Brand, Europhys. Lett. **38**, 341 (1997); Physica (Amsterdam) **117D**, 95 (1998).
[7] C. Crawford and H. Riecke, Physica (Amsterdam) **129D**, 83 (1999).
[8] L. S. Tsimring and I. S. Aranson, Phys. Rev. Lett. **79**, 213 (1997).
[9] S. C. Venkataramani and E. Ott, Phys. Rev. Lett. **80**, 3495 (1998).
[10] W. S. Edwards and S. Fauve, Phys. Rev. E **47**, 788 (1993).
[11] H. Arbell and J. Fineberg, Phys. Rev. Lett. **81**, 4384 (1998).
[12] S. Fauve, *Hydrodynamics and Nonlinear Instabilities,* edited by C. Godreche and P. Manneville (Cambridge University Press, Cambridge, England, 1998).
[13] H. Arbell and J. Fineberg, Phys. Rev. Lett. **84**, 654 (2000).
[14] A. Kudrolli and J. P. Gollub, Physica (Amsterdam) **123D**, 99 (1998).
[15] M. Silber and M. R. E. Proctor, Phys. Rev. Lett. **81**, 2450 (1998).
[16] E. D. Wilkes and O. A. Basaran, J. Fluid Mech. **393**, 333 (1999).
[17] A. D. Myshkis, V. G. Babskii, N. D. Kopachevskii, L. A. Slobozhanin, and A. D. Tyuptsov, *Low-Gravity Fluid Mechanics* (Springer-Verlag, Berlin, 1987).
[18] C. L. Goodridge, W. T. Shi, H. G. E. Hentschel, and D. P. Lathrop, Phys. Rev. E **56**, 472 (1997).
[19] G. D. Crapper, J. Fluid Mech. **2**, 532 (1957).
[20] B. W. Zeff, J. Fineberg, and D. P. Lathrop, Nature (London) **403**, 401 (2000).
[21] M. Rein, J. Fluid Mech. **306**, 145 (1996).
[22] W. C. Macklin and P. V. Hobbs, Science **166**, 107 (1969).